JMEPEG (2009) 18:378–384
DOI: 10.1007/s11665-008-9304-7

1059-9495/$19.00

# Texture Evolution in a Warm-Rolled Ti-IF Steel During Cold Rolling and Annealing

*Yanhui Guo, Zhaodong Wang, Jishan Xu, Guodong Wang, and Xianghua Liu*

*(Submitted December 25, 2007; in revised form July 15, 2008)*

**The texture characteristics of a Ti-IF steel in ferritic hot-rolled (warm-rolled), cold-rolled, and annealed status were studied. The hot bands were obtained by finish rolling in ferrite region, coiling at very low temperature, and then directly annealing in industrial trial. It was found that {001}⟨110⟩ dominates at the surface and {111}⟨112⟩ is the main component at the midsection in the hot band. The α-fiber at the surface as well as at the midsection intensifies during cold rolling and weakens during annealing, while the changing of γ-fiber depends on the hot band texture during cold rolling, but it absolutely intensifies after a well-advanced state of annealing. Orientations concentrate on {001}⟨110⟩ increasingly at the surface and continuously rotate to RD-fiber at the midsection as the reduction increases. The average plastic strain ratio, elongation, and strain hardening exponent measured for the cold-rolled and annealed steel increased with improving annealing temperatures.**

**Keywords** annealing, cold rolling, ferrite region, texture, Ti-IF steel

## 1. Introduction

Interstitial free (IF) steels have been widely used particularly in car body panels due to their excellent formability. It has long been recognized that the presence of favorable texture component in IF steels is responsible for their excellent deep drawability, and it is well known that strong {111} and weak {001} components parallel to the sheet plane produce good formability. Recently, attention has been focused on the improvement of the final product through proper control of the hot-rolling parameters (Ref 1-7). An important result hereby was that hot rolling in the ferrite region, followed by cold rolling and annealing, results in a much stronger γ-fiber than conventional austenite rolling. Most of the papers (Ref 1, 5-7) were concerned with the deep drawability of hot bands. The influence of the chemical composition on the deep drawability of hot bands has been investigated in detail, and the elimination of carbon in solution was reported to be an essential condition for obtaining a high *r* value of hot bands (Ref 8-10). Another important finding was that the texture in the direction of the sheet thickness was varied due to the friction between a roll and a in α-region hot-rolled sheet, and the texture formed in the vicinity of the surface was not favorable for the deep drawability (Ref 11, 12). The other important influential factors on the deep drawability of hot bands, such as rolling temperature, precipitation, have also been investigated (Ref 13, 14). However, few reports dealt with the texture evolution during cold rolling and annealing after ferritically hot rolling (Ref 2). In this paper, special attention has been paid to the formation of texture throughout the rolling and annealing processes.

**Yanhui Guo, Zhaodong Wang, Guodong Wang,** and **Xianghua Liu**, The State Key Laboratory of Rolling and Automation of Northeastern University, Shenyang 110004, P.R. China; and **Jishan Xu**, Jinan Iron and Steel Corp., Jinan, China. Contact e-mail: gyh415@126.com.

## 2. Experimental Procedures

The chemical composition of the steel studied in this work is given in Table 1. The steel slab was austenitized at 1050 °C for 1 h and then it was hot rolled. The finish-rolling temperature was 767 °C and the final thickness of the slab was 5 mm. The amount of deformation during warm rolling is 80%. After laminar cooling (cooling rate was about 30 °C/s), the hot band was coiled at 440 °C and then annealed at 740 °C for 4 h in industrial trial, and its final thickness was 5 mm. The hot band was cold rolled with different reductions to a final slab thickness of 4, 3, 2, 1.5, and 1.25 mm, using a two-high rolling mill and with light oil lubrication. The steels of 1.25 mm were annealed in a special atmosphere furnace to simulate batch annealing. The three annealing temperatures employed in this work were 600, 700, and 750 °C, and the annealing time was 1 h.

Standard metallographic procedures were employed to prepare samples for optical microscopy in the hot-rolled, hot-rolled and annealed, and in the cold-rolled (the sample with 75% reduction was selected) and annealed conditions. Optical microscopy was carried out on the longitudinal (RD-ND) sections.

Texture measurements were conducted after hot rolling and direct annealing, cold rolling, and annealing by X-ray diffraction using a Philips X'PERT Pro MRD system. Orientation distribution functions (ODF) of the global structure were calculated using two-step method with $l_{max} = 16$ based on the series expansion method proposed by Roe (Ref 15) from three incomplete pole figures of {200}, {110}, and {211} and expressed using φ = 45° ODF sections. Experimental background and defocusing corrections were applied by measuring

**Table 1 Chemical composition of the test steel (mass contents in %)**

| Steel grade | C | Si | Mn | P | S | Ti | Nb | N | Als |
|---|---|---|---|---|---|---|---|---|---|
| Ti-IF steel | 0.004 | 0.015 | 0.12 | 0.007 | 0.007 | 0.068 | <0.005 | 0.0028 | 0.034 |

the texture of a pure iron random sample. To illustrate the presence of various textures, the so-called skeleton plots were constructed from the ODF data. These plots describe the preferred crystallographic orientations in the rolling direction (RD//⟨110⟩, α-fiber), normal direction (ND//{111}, γ-fiber), and transverse direction (TD//⟨110⟩, ε-fiber). Specimens for these measurements were taken from the surface and the center thickness.

The mechanical properties including tensile strength, elongation, plastic strain ratio, and strain hardening exponent along three directions of the plate were determined by tensile test on a universal tester at a strain rate of 3 mm/min, and the average values were calculated. Specimens with a gage length of 50 mm and a width of 12.5 mm were used.

## 3. Results

### 3.1 Microstructure

The optical micrographs of samples in the hot-rolled and annealed status, cold-rolled status, and annealed status are given in Fig. 1. After hot rolling and coiling, deformation bands are the main microstructure features, as shown in Fig. 1 (a). It is evident that the majority of grains are elongated along rolling direction in the center of the sample after hot rolling and annealing. The optical micrograph in Fig. 1(c) shows that after cold rolling to a large reduction, the grains cannot be discerned, and the obvious characteristics of the cold microstructure is the formation of the in-grain bands denoted by the postil. The in-grain bands which are described as fish bone by other authors (Ref 16), are vivid in the cold-rolled microstructure of the steel in this work. As shown in Fig. 1(d-f), there are more equiaxed grains present after cold rolling and annealing than after hot rolling and annealing. There are small equiaxed grains embedded in large grains after annealing at 600 °C. With the temperature increasing to 700 °C, more and larger equiaxed grains form, but there are still some small equiaxed grains embedded in large grains. After annealing at 750 °C, a mixture of small and large grains dominates.

### 3.2 Texture

**3.2.1 Texture at the Surface.** The φ = 45° ODF sections of texture at the surface are shown in Fig. 2, and the corresponding intensity changes of ε-fiber (⟨110⟩//TD), α-fiber (⟨110⟩//RD) and γ-fiber (⟨111⟩//ND) are also shown in Fig. 3. As shown in Fig. 2(a), the hot band texture mainly consists of the α-fiber and the γ-fiber. The α-fiber starts at {00l}⟨110⟩ and spreads toward {110}⟨110⟩. {114}⟨110⟩ is the strongest component of the hot band texture with an intensity of about 5× random intensity (RI). The strongest component in γ-fiber is {111}⟨110⟩, the intensity of which is about 4× RI. After cold rolling, as illustrated in Fig. 2(b-f), orientations in α-fiber begin to rotate toward {00l}⟨110⟩, and γ texture intensity decreases with the increase of reduction. The maximum of the ε-fiber deviates 5° from {111}⟨112⟩, locating at (ψ, θ, φ) = (0°, 60°, 45°). All the cold-rolled textures consist of partial α-fiber and weak γ-fiber. The {001}⟨110⟩ component is intensified to 16× RI as the cold reduction is up to 75%, and is always the strongest component after cold rolling in different reductions, consistent with the result of Tóth et al. (Ref 17) that the {001}⟨110⟩ component is inherited from the hot band and its intensity increases with deformation. After annealing at three different temperatures, the change of texture is not absolutely the same, but one common trend is that the intensity of γ-fiber increases and that of partial α-fiber ({001} ~ {223}⟨110⟩) decreases enormously. It can be seen from Fig. 3(a) that the intensity of {001}⟨110⟩ decreases from 16× RI (cold rolled to 75%) to about 2× RI (after annealing). The textures of samples annealed at 700 °C display the same character as that annealed at 600 °C except that the intensity is higher. The intensity of {111}⟨112⟩ component improves from 4.6× RI (after annealing at 600 °C) to 7.5× RI (after annealing at 700 °C) and that of {111}⟨110⟩ from 4× RI to 6.5× RI with the annealing temperature increasing from 600 to 700 °C, as shown in Fig. 3 (c). The change of texture is different after annealing at 750 °C in that {111}⟨112⟩ weakens and {111}⟨110⟩ intensifies, resulting in higher intensity of {111}⟨110⟩ component than that of {111}⟨112⟩ component.

**3.2.2 Texture at the Midsection.** The φ = 45° ODF sections at the midsection are shown in Fig. 4, and the corresponding texture intensities of ε-fiber (⟨110⟩//TD), α-fiber (⟨110⟩//RD), and γ-fiber (⟨111⟩//ND) are shown in Fig. 5. The most prominent texture intensity is along the γ-fiber and the maximum is at {111}⟨112⟩ with an intensity of about 12× RI at the midsection of the hot band. All other texture intensities are quite low, as Fig. 4(a) illustrated. We can see from Fig. 4(b-f) that after cold rolling, orientations rotate toward α-fiber and {001}⟨110⟩ first intensifies at low cold-rolling reduction and gradually spreads all over the α-fiber as the reduction increases. The intensity of γ texture (including {111}⟨110⟩) is reduced, α-fiber (except {111}⟨110⟩ component) is intensified, and the peak in the α-fiber is broad and extends toward {223}⟨110⟩ and {112}⟨110⟩ with an intensity of 8× RI. This indicates that grains with γ orientation rotate to α orientation, leading to high intensity of α-fiber. As shown in Fig. 4(g), after annealing at 600 °C, the intensities of both γ-fiber and α-fiber drop and only the components between {554}⟨225⟩ and {110}⟨001⟩ in the ε-fiber intensify. The textures in γ-fiber stretch from {111}⟨110⟩ to {111}⟨112⟩, with a relatively strong {111}⟨112⟩ component. With increasing temperature, the intensity of γ-fiber and components between {112}⟨110⟩ and {332}⟨110⟩ in the α-fiber improves. All orientations tend to rotate to γ-fiber, giving rise to sharper γ-fiber. The orientation with maximum intensity has clearly shifted from {554}⟨225⟩ toward {111}⟨112⟩. In the TD-fiber, the highest intensity is at {111}⟨112⟩, which is known to be the most stable orientation in this fiber. When the annealing temperature increases to 750 °C, the change is more rapid and the intensity of the strongest component {111}⟨112⟩ reaches 15× RI, only 1× RI higher than that of {111}⟨110⟩, resulting in a uniform γ-fiber, which is favorable to improve plastic strain ratio $r$ value and reduce planar anisotropy exponent $\Delta r$.

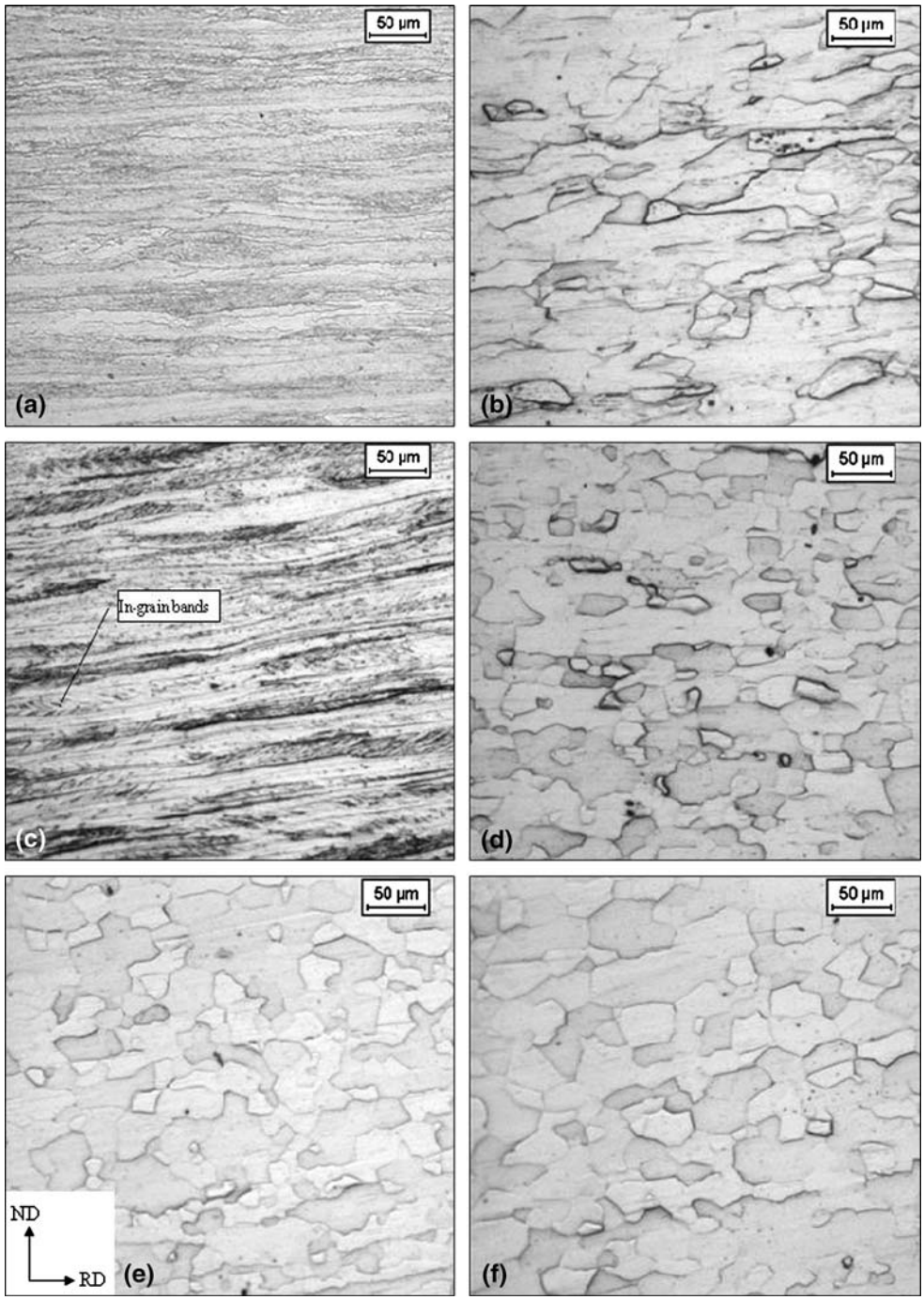


**Fig. 1** Optical micrographs of samples in different conditions: (a) hot rolled; (b) hot rolled and annealed; (c) cold rolled (75%); (d) annealed at 600 °C ; (e) annealed at 700 °C ; and (f) annealed at 750 °C

### *3.3 Mechanical Properties*

The mechanical properties are shown in Fig. 6 and 7. The average values are obtained from that of rolling direction, vertical to rolling direction, and 45° with rolling direction. It is evident that the tensile strength decreases and $r$ value, $n$ value, and elongation increase with increasing annealing temperature. This is related to the texture of the steel. It is well established that $r$ value increases with the {111}/{001} intensity ratio. It is clear from Fig. 2-5 that the intensity of {001} is at the RI and the intensity of {111} increases with the annealing temperature. Therefore, $r$ value increases with the intensity of {111} or, in other words, with the annealing temperature.

## 4. Discussion

It is clear from the above results that the texture characteristic at the surface is absolutely different from that at the midsection in the hot-rolled, as well as in the cold-rolled and annealed, conditions. This difference between the surface and

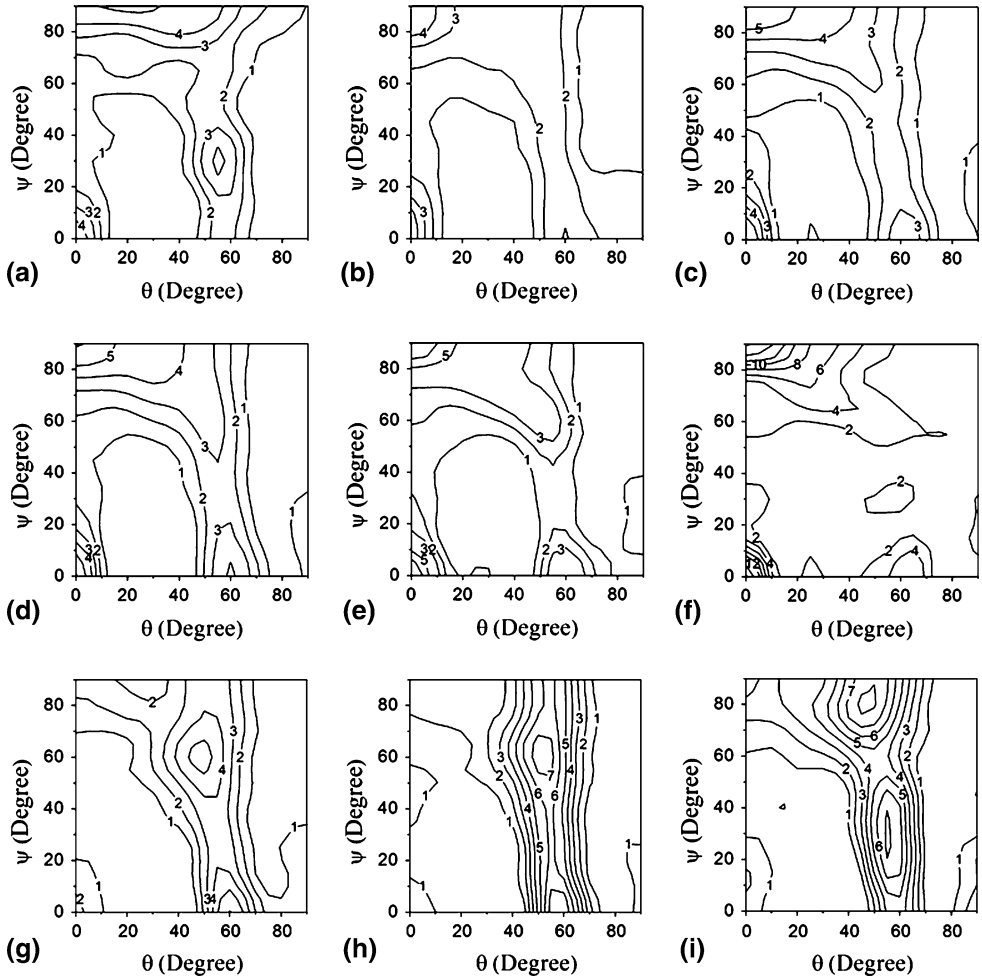


**Fig. 2** φ = 45° ODF sections of texture at the surface in the following conditions: (a) hot rolled and annealed, (b) cold rolled 20%, (c) cold rolled 40%, (d) cold rolled 60%, (e) cold rolled 70%, (f) cold rolled 75%, (g) annealed at 600 °C , (h) annealed at 700 °C , and (i) annealed at 750 °C

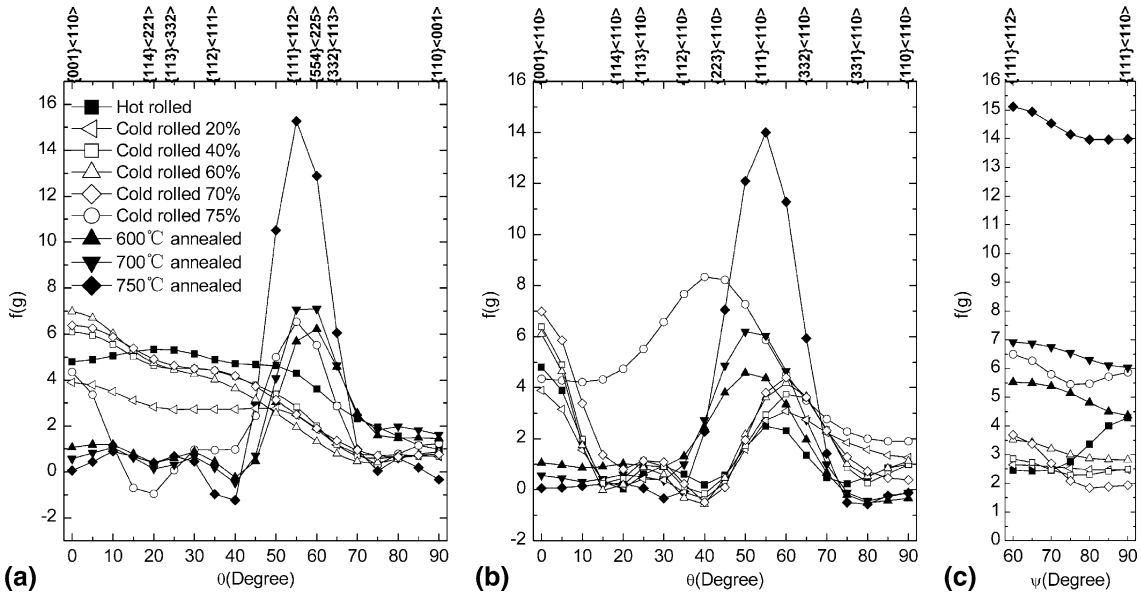


**Fig. 3** Intensity distribution along (a) ε fiber, (b) α fiber, and (c) γ fiber at the surface

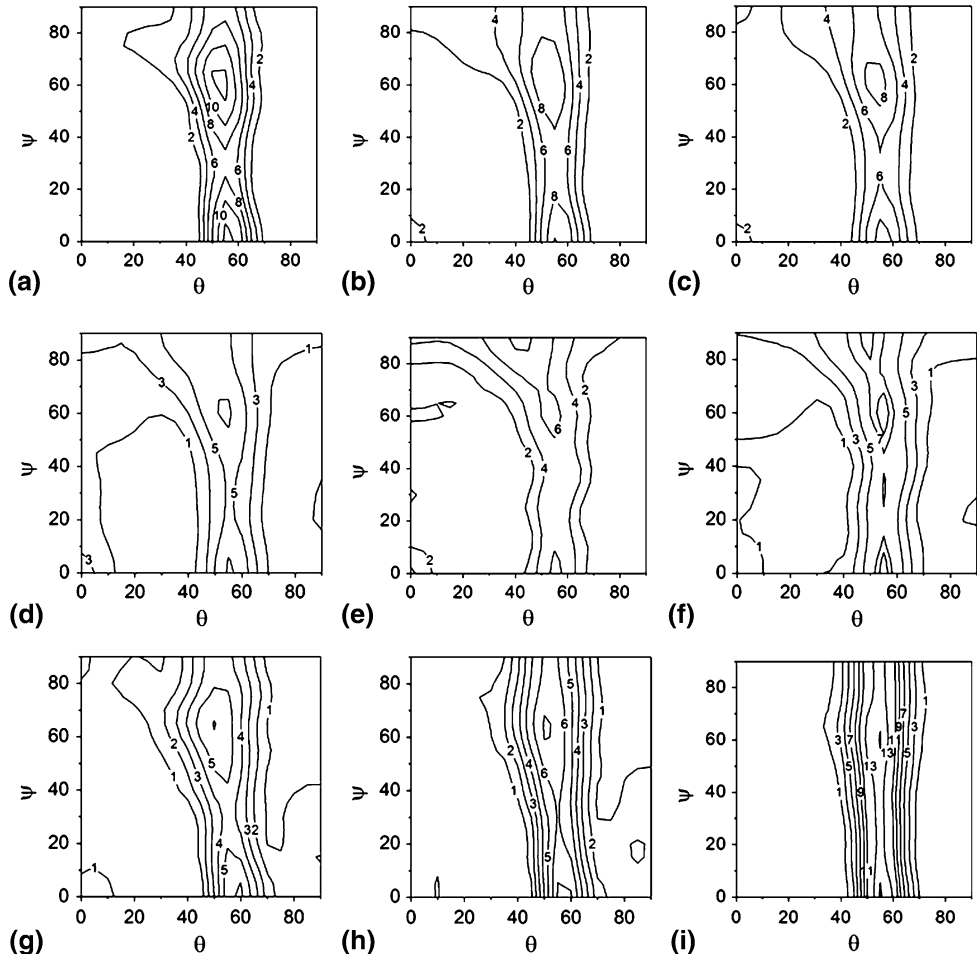


**Fig. 4** φ = 45° ODF sections of texture at the midsection in the following conditions: (a) hot rolled and annealed, (b) cold rolled 20%, (c) cold rolled 40%, (d) cold rolled 60%, (e) cold rolled 70%, (f) cold rolled 75%, (g) annealed at 600 °C , (h) annealed at 700 °C , and (i) annealed at 750 °C

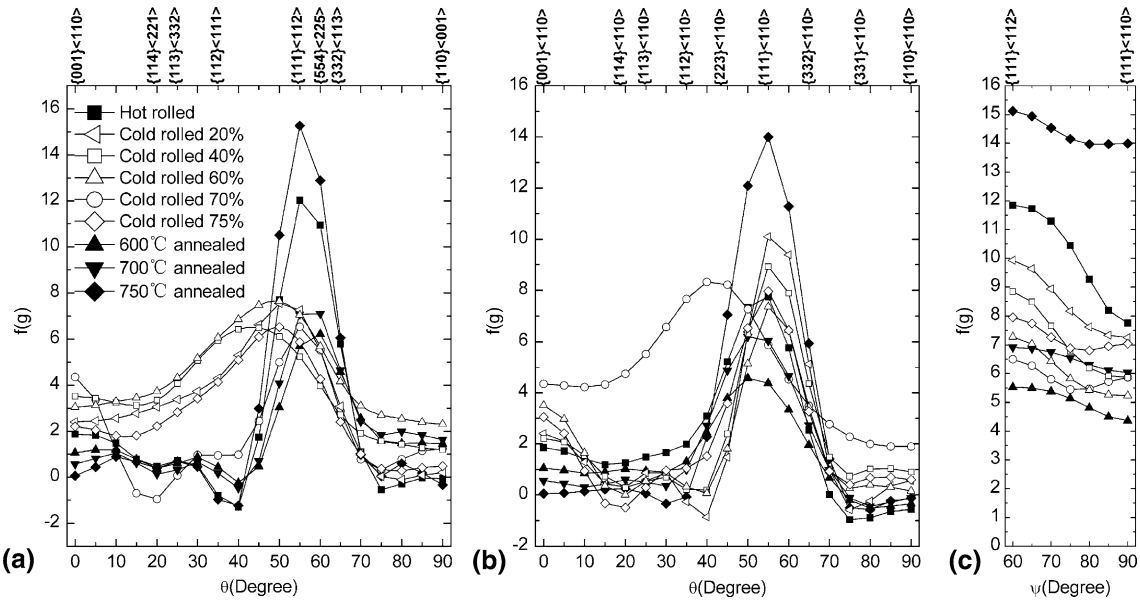


**Fig. 5** Intensity distribution along (a) ε fiber, (b) α fiber and (c) γ fiber at the midsection

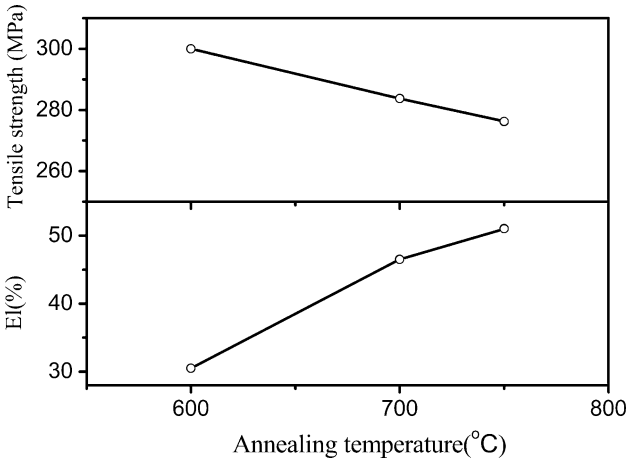


**Fig. 6** Average tensile strength and elongation of samples

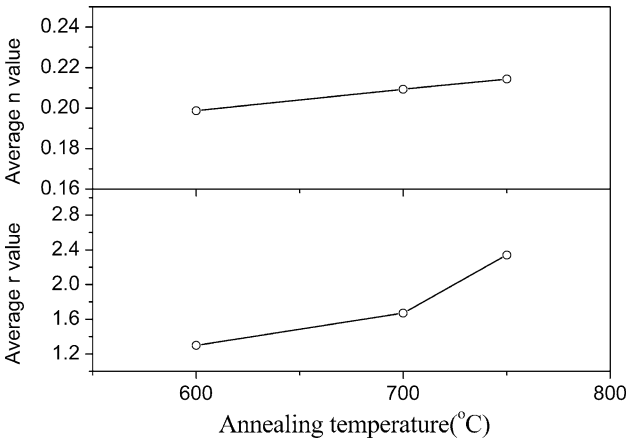


**Fig. 7** Average plastic strain ratio $r$ value and strain hardening exponent $n$ value of samples

the midsection in the hot-rolled condition should be ascribed to the additional shear stress due to the friction between the material and the rolls. Since the shear stress is distributed inhomogenously along the thickness direction, grains at different layers are subject to different stress state and thus rotate variously, leading to distinct texture characteristics at different layers. Furthermore, this difference between the surface and the midsection occurs because of the heredity of textures that shows that the nature and strength of the texture in the cold-rolled and annealed steels are determined by the hot band texture.

The $\{001\}\langle 110\rangle \sim \{111\}\langle 110\rangle$ textures are the main components at the surface of the hot band and the intensity of α texture increases and that of γ texture decreases a little after cold rolling. The development of cold-rolling textures in low and extra low carbon steels has been dealt with in detail by Tóth et al. (Ref 17). They predicted the stability of the main rolling texture components analytically, using a rate dependent theory for mixed $\{112\}\langle 111\rangle$ and $\{110\}\langle 111\rangle$ slip. Both full constraint (Taylor) and relaxed constraint (lath and pancake) grain interaction models (Ref 18-20) were employed for this purpose. This indicates that $\{001\}\langle 110\rangle \sim \{223\}\langle 110\rangle$ is a fairly stable orientation, and that is why its intensity increases during subsequent cold rolling.

Several studies have suggested that texture developed in the hot bands has a great effect on the nature and strength of the texture in the cold-rolled and annealed steels (Ref 21, 22). In the present study, the main texture at the midsection of the hot bands comprises a complete γ-fiber. The γ orientation shifts toward α orientation during cold rolling, in agreement with the results of Inagaki (Ref 23), who concludes that crystal rotates along two paths, one of which is $\{110\}\langle 001\rangle \rightarrow \{554\}\langle 225\rangle \rightarrow \{111\}\langle 112\rangle \rightarrow \{111\}\langle 110\rangle \rightarrow \{223\}\langle 110\rangle$. This indicates γ-fiber is not necessarily intensified during cold rolling. After annealing at 750 °C, there is a complete and uniform γ-fiber stretching from $\{111\}\langle 112\rangle$ to $\{111\}\langle 110\rangle$ and the intensity of α-fiber (except $\{111\}\langle 110\rangle$ component) drops appreciably to RI. This could be regarded as an evidence of full recrystallization at 750 °C, for it is well known that a strong texture in the γ-fiber extending from $\{111\}\langle 110\rangle$ to $\{111\}\langle 112\rangle$ is developed by the well-advanced recrystallization of ferrite during annealing (Ref 24).

As described in Ref 25, the intensity of the $\{001\}\langle 110\rangle$ texture components seems to correlate with the degree of recrystallization of ferrite. When the ferritic grains were mainly unrecrystallized, high intensities of $\{001\}\langle 110\rangle$ were obtained (in surface). When the grains were mainly recrystallized after ferritic rolling, the detrimental rotated cube component, $\{001\}\langle 110\rangle$, was practically nonexistent (at the midsection). This can be explained by the result of Vanderschueren et al. (Ref 16) who have studied the recrystallization in Ti-IF steel with EBSD. They show that the texture of the early nuclei consists of a γ-fiber and α-fiber grains are consumed only after 70% of the material is recrystallized. A strong increase in this texture component is caused by cold rolling, with its intensity increasing from 8 to 16× RI, showing its stability during cold rolling. However, it transforms to γ-fiber during subsequent annealing according to Lee's theory (Ref 26). The $\{001\}\langle 110\rangle$ texture transforms to $\{111\}$ texture by the strain energy release maximization (SERM) model for recrystallization texture, in which the absolute maximum internal stress direction in the deformed state tends to be parallel to the minimum Young's modulus direction of recrystallized grains (Ref 27, 28).

Another result worthy of note is that the intensity of γ-fiber at the midsection after annealing at 600 °C decreases when compared to that after cold rolling. The same result has been reported by Tiitto et al. (Ref 25). A usual observation is that the intensity of γ-fiber is higher after annealing than that in the cold-rolled condition. It has been suggested that the α-fiber will superimpose with the $\{111\}$ intensities in the γ-fiber during recrystallization. The γ-fiber intensities increase during recrystallization and, therefore, are at a higher level in the annealed steels than in the cold-rolled steels. In the present study, we can conclude from the results that, if the steels were recrystallized to a great extent during annealing, the $\{111\}$ intensities would be higher than in the cold-rolled steels (750 °C), whereas partial recrystallization would lead to lower levels than in the cold-rolled condition (600 °C). This observation also suggests that the γ-fiber intensities in the present steel decrease during early stages of recrystallization and start increasing when the recrystallization is well advanced. It is known that during annealing of the deformed ferrite, the grains with γ-fiber intensities, having high stored energy, are likely to recrystallize early at a high rate (Ref 16, 24). The grains with the rotated cube orientation, $\{001\}\langle 110\rangle$, are quite stable and are consumed only during the later stages of recrystallization. The decrease of the $\{001\}\langle 110\rangle$ components in the surface of

annealed steel, having been very prominent after the cold rolling, indicates that the ferrite has undergone extensive recovery and recrystallization, removing this orientation during annealing.

## 5. Conclusions

The following general conclusions based on the results of this work can be drawn.

- Texture characteristic at the surface is absolutely different from that at the midsection in the hot-rolled and direct annealed as well as in the cold-rolled and annealed steels.
- With increasing annealing temperature, the intensity of {111} texture improves, and as a result, *r* value increases.
- α-fiber at the surface as well as at the midsection intensifies during cold rolling and weakens during annealing, while the changing of γ-fiber is not stationary during cold rolling, but it absolutely intensifies after a well-advanced state of annealing. To obtain a high {111} texture intensity in the cold-rolled and annealed condition, the annealing must result in a well-advanced state of recrystallization.


### Acknowledgment

The authors are grateful to the National Natural Science Foundation of China for financial support, under Grant No. 50104004.


### References


1. T. Andreas and K. Radko, Ferritic Rolling with Additional Annealing to Produce a Deep-Drawable Ultra-Thin-Gauge Hot Strip, *Steel Res.*, 2000, **71**(12), p 497–503
2. V.J. Martinez, J.I. Verdeja, and J.A. Pero-Sanz, Interstitial Free Steel: Influence of α Phase Hot-Rolling and Cold-Rolling Reduction to Obtain Extra-Deep Drawing Quality, *Mater. Charact.*, 2001, **46**(1), p 45–53
3. P. Juntunen, D. Raabe, P. Karjalainen, T. Kopio, and G. Bolle, Optimizing Continuous Annealing of Interstitial-Free Steels for Improving Deep Drawability, *Metall. Mater. Trans*, 2001, **32A**(8), p 1989–1995
4. L.K. Tung, M.Z. Quadir, and B.J. Duggan, A Novel Rolling-Annealing Cycle for Enhanced Deep Drawing Properties in IF Steels, *Key Eng. Mater.*, 2002, **233–236**(I), p 437–442
5. T. Andreas and K. Radko, Deep-drawable thin-gauge hot strip of steel as a substitution for cold strip, *ISIJ Int.*, 2000, **40**(9), p 927–931
6. Z.D. Wang, Y.H. Guo, Z. Zhao, and D.Q. Sun, 应用铁素体区热轧工艺开发超低碳热轧深冲板 (Developing an Ultra-Low Carbon Deep-Drawing Sheet Steel by Ferritic Hot Rolling Process), *J. Northeastern Univ.*, 2005, **26**(8), p 747–750 (in Chinese)
7. H. Zhao, S.C. Rama, G.C. Barber, Z. Wang, and X. Wang, Experimental Study of Deep Drawability of Hot Rolled IF Steel, *J. Mater. Process. Technol.*, 2002, **128**(1–3), p 73–79
8. T. Senuma, H. Yada, R. Shimizu, and J. Harase, Textures of Low Carbon and Titanium Bearing Extra Low Carbon Steel Sheets Hot Rolled Below Their $A_{R3}$ Temperatures, *Acta Metall. Mater*, 1990, **38** (12), p 2673–2681
9. Y. Chen, X. Chen, C.Y. Li, X.Y. Li, and Y.L. Kang, Effect of Chemical Composition and Processes on the Texture of Hot-Rolled Deep Drawing Steel Sheet, *Acta Metall. Sinica*, 2002, **15**(3), p 324–330
10. M.D. Nave, M.R. Bsrnett, and H. Beladi, The Influence of Solute Carbon in Cold-rolled Steels on the Shear Band Formation and Recrystallization Texture, *ISIJ Int.*, 2004, **44**(6), p 1072–1078
11. C.J. Barrett, Influence of Lubrication on Through Thickness Texture of Ferritically Hot Rolled Interstitial Free Steel, *Ironmaking Steelmaking*, 1999, **26**(5), p 393–397
12. S. Matsuoka, M. Morita, O. Furukimi, and T. Obara, Effect of Lubrication Condition on Recrystallization Texture of Ultra-Low C Sheet Hot-Rolled in Ferrite Region, *ISIJ Int.*, 1998, **38**(6), p 633–639
13. M.R. Toroghinejad, A.O. Humphreys, D.S. Liu, F. Ashrafizadeh, A. Najafizadeh, and J.J. Jonas, Effect of Rolling Temperature on the Deformation and Recrystallization Textures of Warm-Rolled Steels, *Metall. Mater. Trans.*, 2003, **34A**(5), p 1163–1174
14. X.J. Guan, Y. Li, and Z.C. Wang, 铁素体区热轧Ti-IF钢的析出物研究 (Research on Precipitation of Hot Rolled Ti-IF Steels in the Ferrite Region), Iron Steel, 2004, **39**(9), p 58–60 (in Chinese)
15. R.Y. Roe, Description of Crystallite Orientation in Polycrystalline Materials. III General Solution to Pole Figure Inversion, *J. Appl. Phys.*, 1965, **36**(6), p 2024–2031
16. D. Vanderschueren, N. Yoshinaga, and K. Koyama, Recrystallization of Ti IF Steel Investigated with Electron Back-Scattering Pattern (EBSP), *ISIJ Int.*, 1996, **36**(8), p 1046–1054
17. L.S. Tóth, J.J. Jonas, D. Dnaiel, and R.K. Ray, Development of Ferrite Rolling Textures in Low- and Extra Low-Carbon Steels, *Metall. Trans.*, 1990, **21A**(11), p 2985–3000
18. J.L. Raphanel and P.V. Houtte, Simulation of the Rolling Textures of B. C.C. Metals by Means of the Relaxed Taylor Theory, *Acta Metall.*, 1985, **33**(8), p 1481–1488
19. M. Arminjon, Theory of a Class of Heterogeneous Taylor Models. Application to Deformation Textures of Steels, *Acta Metall.*, 1987, **35**(3), p 615–630
20. P. Gilormini, The Theory of Rate Sensitive Pencil Glide Application to Rolling Textures, *Acta Metall.*, 1989, **37**(7), p 2093–2101
21. R.K. Ray, J.J. Jonas, and R.E. Hook, Cold Rolling and Annealing Texture in Low Carbon and Extra Low Carbon Steels, *Int. Mater. Rev.*, 1994, **39**(4), p 129–172
22. Z.C. Wang and X.J. Wang, A New Technology to Improve the *r*-Value of Interstitial-Free Steel Sheet, *J. Mater. Process. Technol.*, 2001, **113** (1–3), p 659–661
23. H. Inagaki, Fundamental Aspect of Texture Formation in Low Carbon Steel, *ISIJ Int.*, 1994, **34**(4), p 313–321
24. Y. Hayakawa and J.A. Szpunar, Modeling of Texture Development During Recrystallization of Interstitial Free Steel, *Acta Mater.*, 1997, **45**(6), p 2425–2434
25. K.M. Tiitto, C. Jung, P. Wrav, C.I. Garcia, and A.J. Deardo, Evolution of Texture in Ferritically Hot Rolled Ti and Ti + Nb Alloyed ULC Steels during Cold Rolling and Annealing, *ISIJ Int.*, 2004, **44**(2), p 404–413
26. D.N. Lee, Evolution of Recrystallization Textures from Deformation Textures, *Scr. Metall. Mater.*, 1995, **32**(10), p 1689–1694
27. S. Hong and D.N. Lee, Recrystallization Textures in Cold-Rolled Ti Bearing IF Steel Sheets, *ISIJ Int.*, 2002, **42**(11), p 1278–1287
28. Y.B. Park, L. Kestens, and J.J. Jonas, Effect of Internal Stresses in Cold Rolled IF Steel on the Orientations of Recrystallized Grains, *ISIJ Int.*, 2000, **40**(4), p 393–401